Published as: *Nat Neurosci*. 2014 December ; 17(12): 1830–1839.

A genetically specified connectomics approach applied to long-range feeding regulatory circuits

Deniz Atasoy[1,2,3,*], **J. Nicholas Betley**[1], **Wei-Ping Li**[1], **Helen H. Su**[1], **Sinem M. Sertel**[2], **Louis K. Scheffer**[1], **Julie H. Simpson**[1], **Richard D. Fetter**[1,*], and **Scott M. Sternson**[1,*]

[1]Janelia Farm Research Campus, HHMI, 19700 Helix Dr. Ashburn, VA 20147 USA

[3]Research center for regenerative and restorative medicine (REMER)

Abstract

Synaptic connectivity and molecular composition provide a blueprint for information processing in neural circuits. Detailed structural analysis of neural circuits requires nanometer resolution, which can be obtained with serial section electron microscopy. However, this technique remains challenging for reconstructing molecularly defined synapses. We used a Genetically Encoded Synaptic marker for Electron Microscopy (GESEM) based on intra-vesicular generation of electron-dense labeling in axonal boutons. This approach allowed identification of synapses from Cre recombinase-expressing or GAL4-expressing neurons in the mouse and fly with excellent preservation of ultrastructure. We applied this tool to visualize long-range connectivity of AGRP and POMC neurons in the mouse, two molecularly defined hypothalamic populations important for feeding behavior. Combining selective ultrastructural reconstruction of neuropil with functional and viral circuit mapping, we characterized some basic features of circuit organization for axon projections of these cell types. These experiments demonstrate that GESEM-labeling enables long-range connectomics with molecularly defined cell types.

INTRODUCTION

Brain tissue is densely packed with complex circuits comprised of neurons and other cells, their extensive fine processes, and synapses originating from multiple cell types. These circuits are being described with increased granularity by specifying circuit nodes as molecularly defined cell types, based on gene expression differences between neurons. Consequently, techniques for visualizing neural circuit structures need to be adapted for molecularly defined circuits. A number of genetic approaches have been developed to selectively label and image molecularly defined cell types[1]. Labeled neurons can be

[*]To whom correspondence should be addressed. sternsons@janelia.hhmi.org (S.M.S.), datasoy@medipol.edu.tr (D.A.), fetterr@janelia.hhmi.org (R.D.F), Phone: 571-209-4103, Fax: 571-209-4914.
[2]Current address: Department of Physiology, School of Medicine, Istanbul Medipol University, Istanbul, Turkey

Author Contributions

D.A. and S.M. Sternson designed the experiments and wrote the paper; D.A. and S.M. Sertel analyzed EM images and reconstructed synapses; J.H.S. suggested VAMP2:HRP labeling and generated *UAS-nSyb:HRP* fly line; J.N.B. performed immunohistochemistry and image analysis; H.H.S. performed molecular cloning; R.D.F. developed tissue preparation and staining protocols; W-P.L., R.D.F. performed sectioning and TEM imaging; R.D.F. and L.K.S. performed electron micrograph registration and alignment.

visualized with light microscopy, but this technique lacks the resolution to directly detect synaptic connections because the apparent overlap of axonal and dendritic arbors in light microscopy is often an unreliable predictor of connectivity[2]. New anatomical techniques have made progress towards circumventing these issues, such as super-resolution imaging[3], GFP-reconstitution across synaptic partners[4], and trans-synaptic viral tracing[5]. In addition, functional circuit mapping techniques based on genetically encoded tools for activity manipulation can also be used to probe synaptic connectivity[6,7]. A common characteristic of these methods is that they simplify the context of neural circuit connections by selective visualization of molecularly defined neurons and their connections, while ignoring complex but unlabeled neuropil.

In contrast, nanometer-scale anatomical analysis provides unbiased insight into the organization of neural circuit connections. Ultrastructure imaging by electron microscopy (EM) remains the gold standard to unambiguously identify synapses and also provides detailed cell biological information about the connections, such as postsynaptic density, organelle distribution, and subcellular targeting. Recent studies have demonstrated the feasibility of large-scale reconstruction of mammalian and insect neural circuits using serial section EM[8-10]. Large-scale ultrastructural detection of connections from molecularly defined cell types has lagged due to reliance on antibody detection of antigens that are uniquely present in those cells. In addition, the integrity of membranous structures is challenged during immunodetection due to the need for membrane permeabilization with strong detergents or, in the absence of detergent, confined to surface labeling and tissue cracks[11]. As a result, connectivity analysis for molecularly defined neurons is frequently limited to anecdotal examples.

In principle, these issues can be addressed by genetic labeling methods[12-16]. Expression of horseradish peroxidase (HRP)[14,17] and the engineered singlet oxygen generator (miniSOG)[15] have been used to generate electron contrast in neuronal samples. HRP is not functional when expressed in the cytosol[18], but the enzymatic activity is preserved when it is targeted to the extracellular plasma membrane[14,17] or endoplasmic reticulum[19], and its expression does not perturb basic synaptic ultrastructure[17,19]. HRP and miniSOG expression are visualized through enzymatic oxidation of 3,3′-diaminobenzidine (DAB) in the presence of hydrogen peroxide (as well as light for miniSOG), which generates a polymeric precipitate. Subsequent processing with osmium tetroxide makes this DAB-reaction product electron-dense, which increases electron scattering in transmission electron microscopy (i.e., reduces electron transmission) and appears as a corresponding dark area on the image[20]. However, DAB reaction product can diffuse from the site of production and obscure some ultrastructural details when targeted to the plasma membrane. To address this issue for molecularly defined cell types, we targeted expression of HRP to the lumen of synaptic vesicles. Upon exposure to DAB and hydrogen peroxide, this method labeled the interior of synaptic vesicles, which permitted identification of axonal release sites with minimal tissue processing and excellent ultrastructural preservation.

As a proof-of-principle example of long-range ultrastructure circuit mapping and quantitative analysis of molecularly defined synapses, we investigated neural circuits that control feeding behavior. These circuits involve separate molecularly defined hypothalamic

neuron types as critical circuit nodes with long-range axonal projections that are critical regulators of food seeking and consumption. Two intermingled cell types located in the hypothalamic arcuate nucleus (ARC) are defined by expression of the neuropeptides Agouti related peptide (AGRP) and Proopiomelanocortin (POMC). These cell types have opposite effects on feeding behavior and energy balance[21], where increased electrical activity in AGRP neurons drives food seeking and consumption[22,23], and, conversely POMC neuron activation suppresses food intake[22]. AGRP and POMC neurons have an overlapping axonal projection pattern spanning multiple brain regions, and their axon projections to the paraventricular hypothalamus (PVH) have received particular attention as a key circuit that regulates feeding[24-26]. We investigated the ultrastructure of synapses from AGRP and POMC neurons in combination with channelrhodopsin-assisted functional circuit mapping[6,7] and anterograde transsynaptic viral tracing to dissect these key long-range connections. Good preservation of ultrastructure and efficient labeling enabled us to extract high-resolution reconstructed examples of release sites from these cell types across a large continuous volume. This provides an initial assessment of anatomical features indicative of circuit properties such as the relative utilization of wired and volume neurotransmission, the use of excitatory and inhibitory neurotransmitters, and the localization of their synaptic contacts. Moreover, these experiments demonstrate the practical application of GESEM-labeling techniques in two mouse brains for long-range ultrastructural circuit mapping of molecularly defined cell types.

RESULTS

A genetically encoded synaptic marker for EM

To label axonal release sites in molecularly defined neuron types, we targeted a Genetically Encoded Synaptic marker for Electron Microscopy (GESEM) to the lumen of secretory vesicles. For this, we used a chimeric protein in which horseradish peroxidase (HRP) was fused to the C-terminus of vesicle-associated membrane protein 2 (VAMP2)/ synaptobrevin-2 (Syb2)[27], which localized HRP to the synaptic vesicle lumen (VAMP2:HRP, Fig. 1a). VAMP2 was chosen because of its ubiquitous presence among small clear vesicles as well as large dense core vesicles and was therefore expected to label fast neurotransmitter and peptidergic neuromodulatory release sites, respectively[28]. To achieve cell type-specific expression, we placed the VAMP2:HRP coding sequence in an inverted orientation into a Cre recombinase (Cre)-dependent recombinant adeno-associated virus (rAAV) targeting vector (rAAV2/1-*CAG-FLEX-rev-Vamp2*:HRP)[7]. We tested the validity of this approach in mice by labeling the projections of molecularly defined AGRP and POMC neurons. The Cre-dependent VAMP2:HRP-expressing rAAV was used to transduce AGRP and POMC neurons in the ARC of *Agrp-Cre* or *Pomc-Cre* mice, respectively (Fig. 1b). We focused on the long-range (>1 mm) synaptic connectivity of their axons with neurons in the PVH (Fig. 1b), which receives strong axonal input from the ARC ($ARC^{AGRP}\rightarrow PVH$, $ARC^{POMC}\rightarrow PVH$). Following HRP-catalyzed oxidation of DAB and subsequent processing, electron-dense staining was encapsulated within the vesicular membrane (Fig. 1c,d). This permitted unambiguous identification of the labeled boutons without obscuring other intracellular and extracellular membranes.

To further evaluate the general applicability of this cell-type specific EM labeling approach, we generated a transgenic *Drosophila melanogaster* line, using the fly homolog of *Vamp2* (neuronal synaptobrevin, *nSyb*), for broad neuronal expression of nSyb:HRP (*c155-GAL4;UAS-nSyb:HRP*). Similar to results with mouse brains, we observed synapses labeled by dark, electron-dense vesicles similar in size to the unfilled vesicles (Fig 1e). This technique allowed preservation of cell membranes and key ultrastructural features such as T-bars, which indicate the sites of synaptic contact in flies. Therefore, GESEM-labeling by intravesicular synaptic targeting with VAMP2:HRP allows *in vivo* labeling of release sites from molecularly defined cell types in mouse and fly brains for ultrastructural analysis by electron microscopy.

GESEM-labeling of molecularly defined synapses

We used GESEM-labeling to identify axons and reconstruct synaptic connections of AGRP and POMC neurons in the PVH. After HRP-mediated DAB oxidation and subsequent processing, we prepared serial sections from the PVH and imaged by transmission electron microscopy. For axonal reconstructions, we used two continuous volumes of neuropil (one for each cell type) that were from one *Agrp-Cre* mouse and one *Pomc-Cre* mouse. For analysis of $ARC^{POMC}\rightarrow$PVH axonal boutons, 11933 PVH images were aligned, corresponding to a continuous volume of ~120,000 μm^3 (~200×200×3_μm) (Fig. 2a–c). Preservation of membranous structures enabled three dimensional reconstruction of labeled axons and their boutons (Fig. 2d–g). We observed two types of vesicles that were categorized based on diameter: small vesicles (SV, 35 – 50 nm), and large vesicles (LV, 80 – 130 nm) of varying core density (Fig. 2f). Based on prior immuno-EM analysis[29,30], these likely correspond to fast amino acid neurotransmitter and neuropeptide release, respectively. Most labeled boutons from POMC neurons had ultrastructural characteristics of a synaptic contact (Fig. 2h).

Similarly, for a mouse expressing VAMP2:HRP in AGRP neurons, we imaged and aligned 10808 PVH images corresponding to a continuous volume of ~90,000 μm^3 (Fig. 3a–c). Some boutons that were reconstructed (Fig. 3d–f) showed a mixture of SVs and LVs as well as a synaptic contact (Fig. 3g), while others primarily contained LVs and lacked synaptic contacts (Fig. 3h). Examination of the EM stacks revealed that 32% of identified $ARC^{AGRP}\rightarrow$PVH boutons had a post-synaptic partner (Fig. 3i).

For GESEM-labeling with VAMP2:HRP in both mouse and fly brains, not all vesicles within a bouton were labeled by the DAB reaction. AGRP axonal boutons showed higher penetrance of vesicular DAB labeling (35%) than POMC terminals (13%) (Fig. 4a). In both cell types, the penetrance of labeled vesicles was higher for SVs than LVs (Fig. 4b,c). However, these differences in labeling efficacy have a limited influence on bouton identification because only a few labeled vesicles, typically out of tens to hundreds within a bouton, are sufficient for cell type-specific synapse identification.

Organelle profile within ARC→PVH boutons

The organelle profile of synaptic release sites offers insight into synaptic function for these two circuits. Because GESEM labeling is confined to vesicles, the boutons were spared from

obscuring deposits often seen with other HRP labeling methods, allowing clear visualization of structural details. We selected 51 of the complete boutons from each labeled cell type and analyzed their LV and SV composition (Fig. 5a) and postsynaptic profile (Fig. 5b,c and Supplementary Fig. 1a–d). In the boutons that formed synaptic contacts, SVs were abundant and clustered near the release site; LVs were further away. The number of docked vesicles, a morphological correlate of the readily releasable pool[31], was similar at synapses for both cell types (AGRP = 6.6 ± 0.7, n = 15 boutons from one *Agrp-Cre* mouse; POMC 6.1 ± 0.7, n = 28 boutons from one *Pomc-Cre* mouse; $P > 0.05$, U-test) (Supplementary Fig. 2). A second type of bouton was non-synaptic, in which most of the vesicles were LVs (Fig. 3h) and likely peptidergic based on their similar morphology to other known peptidergic release sites[30,32]. These data show that quantitative analysis of vesicle types in molecularly defined cell types is facilitated by high quality ultrastructural preservation with GESEM-labeling.

Other characteristics of these labeled boutons were also notable. For several boutons, including non-synaptic LV-containing boutons, we also observed the DAB reaction product on the extracellular membrane segments, which is an outcome expected from fusion of VAMP2:HRP-containing vesicles (Supplementary Fig. 3a,b). Furthermore, several membrane invaginations resembling Ω-structures were identified in non-synaptic LV-containing boutons (Supplementary Fig. 3c–h), which can be indicative of vesicle fusion.

Synaptic function is also affected by mitochondria, which influence the energy supply for synaptic transmission as well as calcium buffering during synaptic activation[33]. Therefore, we analyzed the number and distribution of mitochondria in labeled boutons. In our imaged volumes of the PVH, AGRP boutons had fewer mitochondria than POMC boutons (Fig. 5d). The number of mitochondria was correlated with the number of SVs ($r = 0.4$), as would be expected from energetic requirements in the synaptic vesicle cycle (Fig. 5e), but were independent of LV pool size ($r = 0.04$) (Fig. 5f). Consistent with this, we found that boutons with morphological characteristics of a synaptic contact usually contain mitochondria, while a large fraction of non-synaptic neuromodulatory boutons do not (Fig. 5g,h). Therefore, the difference in mitochondria numbers in AGRP and POMC neuron projections is likely due to the lower number of synaptic contacts for $ARC^{AGRP} \rightarrow PVH$ projections (Fig. 2h and 3i). Collectively though, these results demonstrate that GESEM-labeling enables systematic, quantitative, and information-rich analysis of intracellular organelle profiles in boutons from long-range projections of molecularly defined cell types.

Intra-axonal bouton variability

Do synaptic and non-synaptic types of boutons arise from separate neuronal subpopulations? Preservation of ultrastructure in GESEM-labeled samples allowed tracing and reconstruction of axonal segments from molecularly defined cell types within the imaged volume. In our axonal reconstructions, several axon segments had multiple boutons within the imaged volume (11 from AGRP and 6 from POMC, Fig. 5i).

For AGRP axons, both synaptic and non-synaptic boutons were found in the same axons (Fig. 5i). Connected, adjacent boutons often showed striking differences in SV distribution, where SVs were segregated primarily to boutons that formed a synapse (Fig. 5i–l). LV distribution was similar across adjacent synaptic and non-synaptic boutons (Fig. 5i–l).

Therefore, individual ARC^{AGRP}→PVH axons within our imaged volume contain two types of specialized boutons that are either predominantly LV-containing (peptidergic) and non-synaptic or mixed LV/SV (peptide/fast neurotransmitter) synaptic release sites. In contrast, for POMC axons, neighboring boutons had a consistent synaptic or non-synaptic ultrastructure as well as vesicle pool composition (Fig. 5i–k). Thus, these two bouton configurations may arise from separate populations, however analysis in a larger PVH volume and additional animals is required to validate the generality of these observations. Taken together, our analysis demonstrated that GESEM-labeling is also compatible with reconstruction of axons from long-range projections of molecularly defined neurons, which reveals substantial variability within release sites both between and within axonal segments.

Subcellular targeting of ARC→PVH release sites

For fast chemical neurotransmission, the subcellular location of synaptic inputs strongly affects potency to perturb neuron electrical activity[34]. Our measurements revealed that 26% of ARC^{AGRP}→PVH synapses were directly onto somata but this fraction was only 2% for ARC^{POMC}→PVH connections (Supplementary Fig. 4a).

Additional analysis of GESEM-labeled presynaptic terminals showed that 19% of ARC^{POMC}→PVH synapses were onto spines, but none for ARC^{AGRP}→PVH synapses (Supplementary Fig. 4a). We also found that 69% of POMC synapses were onto dendrites <1 μm shaft caliber, but only 9% for AGRP axons (Supplementary Fig. 4a). Because the diameter of PVH dendritic processes decrease with branching and distance from soma[35], this indicates that AGRP synapses onto PVH neuron dendrites may be closer to the soma than POMC synapses. Therefore, within our imaged volumes, reconstructions GESEM-labeled axonal boutons as well as postsynaptic dendrites and somata show a striking difference in subcellular targeting of these molecularly defined circuit connections, although further analysis in larger volumes is required to verify these findings.

Ultrastructural prediction of synaptic sign

The ultrastructural characteristics of synaptic contacts can also be used to predict functional synaptic properties; symmetric synapses are typically inhibitory and asymmetric synapses are excitatory and release glutamate. Because GESEM-labeling results in excellent preservation of synapse ultrastructure, GESEM-assisted reconstructions of boutons and post-synaptic elements clearly reveal the synapse morphology. Using this approach, we found that AGRP neuron synapses in the PVH were mostly symmetric (Fig. 6a,b; symmetric: 22% of release sites; asymmetric: 3%). This result is consistent with previous immuno-EM analysis that showed examples of symmetric AGRP neuron synapses in the PVH[36], however GESEM-labeling and reconstruction facilitates quantitative analysis across populations of these release sites. A majority (52%) of ARC^{AGRP}→PVH boutons lacked evidence of a synaptic contact (Fig. 6a). In addition, a subset of the boutons could not be classified either due to sectioning in the plane of the synaptic contact (*en face*, 7%) or due to damaged sections or imperfect membrane labeling (undetermined, 16%). We verified the results of EM analysis of GESEM-labeled boutons using immunohistochemical/light microscopic investigation of AR^{CAGRP}→PVH axons, which showed that nearly all of the boutons are

peptidergic and that only a subset express the vesicular GABA transporter (vGat), indicating that they are GABAergic (Supplementary Fig. 4b–d).

For POMC neuron release sites in the PVH, we identified asymmetric (32%) and symmetric (20%) synaptic profiles (Fig. 6a,b). These observations were supported using immunohistochemistry/light microscopy, which also indicated that many more POMC neuron axonal boutons were glutamatergic than GABAergic (vesicular glutamate transporter-2-positive: 50%, n = 108 boutons from 2 mice; vGat-positive: 9%, n = 54 boutons from 2 mice) (Supplementary Fig. 4e–g). The area of the postsynaptic density (PSD) reflects synaptic strength of asymmetric synapses[37], and PSD area could be readily determined for GESEM-labeled synapses. For ARC$^{POMC}\rightarrow$PVH synapses, PSD area was significantly less than neighboring asymmetric synapses in the PVH (POMC: 0.098 ± 0.01 μm^2, n = 11 boutons from one mouse; other PVH: 0.17 ± 0.03 μm^2, n = 15 boutons from one mouse; U-test, $P = 0.02$). In addition, a subset (24%) of reconstructed ARC$^{POMC}\rightarrow$PVH boutons lacked evidence of a synaptic contact (Fig. 6a). Therefore, based on a limited volume of the PVH, our initial evaluation of ARC$^{POMC}\rightarrow$PVH projections suggests that they are heterogeneous and primarily form weak, excitatory synaptic connections. Taken together, this analysis shows that the preservation of high quality ultrastructure enables systematic characterization of synaptic morphology across a volume containing many synapses from molecularly defined cell types.

Functional evaluation of ARC→PVH projections

To complement investigation of the ultrastructure of ARC$^{AGRP}\rightarrow$PVH and ARC$^{POMC}\rightarrow$PVH projections, we sought to extend our circuit analysis using a functional approach with cell type-specific channelrhodopsin-assisted circuit mapping[6,7] (Supplementary Fig. 5a). For ARC$^{POMC}\rightarrow$PVH, we observed a low incidence of synaptic currents (3/66 PVH neurons from 14 mice; glutamatergic: 2, GABAergic: 1; Supplementary Fig. 5b-c), even under elevated synaptic release probability conditions (see Methods). Sporadic detection of functional connections and their low amplitude are likely due, in part, to the tendency for weak POMC synapses, consistent with small PSD area, to form onto electrotonically distant sites from the somatic recording electrode, which is in agreement with the GESEM-assisted observation of small caliber dendritic segments being synaptic targets (Supplementary Fig. 4a).

For ARC$^{AGRP}\rightarrow$PVH circuits, we have reported previously that nearly half of PVH neurons receive GABA-mediated synaptic input from AGRP neurons[24] (Supplementary Fig. 5b–c). We estimated the mean number of AGRP neuron synapses contacting PVH neurons from the ratio of the maximal optically evoked ARC$^{AGRP}\rightarrow$PVH synaptic current amplitude (724 ± 152 pA, n = 11 neurons from 4 mice) to unitary current amplitudes from desynchronized evoked release (54.2 ± 5 pA, n = 12 neurons from 4 mice, Supplementary Fig. 5d). This indicates ~13 ARC$^{AGRP}\rightarrow$PVH synapses per connected neuron, which is consistent with prior anatomical reports of AGRP boutons clustered around PVH neurons[36]. Minimal optogenetic stimulation[38] showed lower average IPSC amplitude (164 ± 25 pA, n = 7 neurons from 5 mice, Supplementary Fig. 5d,e) than maximal stimulation, but IPSCs were larger than the average unitary amplitude, indicating that individual AGRP axons can form

multiple synapses onto PVH neurons. These functional data, taken together with ultrastructural observations of synapse subcellular localization, show that strong inhibition by $ARC^{AGRP}\rightarrow$PVH projections involves multiple AGRP axons per cell, which often form several synapses around PVH neuron somata and proximal dendrites.

Convergence AGRP and POMC synaptic inputs

Ultrastructure analysis of GESEM-labeled PVH tissue indicates that different subcellular postsynaptic compartments are targeted by AGRP and POMC projections. However, since our neuronal reconstructions are based on limited volumes from two different animals, it is not possible with these data sets to distinguish whether these two cell types can target the same postsynaptic PVH neurons.

To examine the possibility of convergence of AGRP and POMC synaptic input on PVH neurons, we employed a strategy to first label $ARC^{POMC}\rightarrow$PVH postsynaptic neurons and then to identify juxtaposed AGRP boutons. A Cre-dependent herpes simplex virus (HSV) anterograde transsynaptic tracer, HSV129(ΔTK)-loxP-STOP-loxP-*tdtomato:2a:TK* (H129ΔTK-TT)[39], was injected into the ARC of *Pomc-Cre* mice, which resulted in tdtomato expression in POMC neurons and, through transsynaptic transfer, in other ARC neurons (Supplementary Fig. 6a,b). Because AGRP neurons are a major presynaptic source of input to POMC neuons[24], we checked for evidence of unwanted retrograde transfer by inspecting AGRP boutons, which did not show tdtomato expression (Supplementary Fig. 6a,c), in line with prior evidence of selective anterograde transsynaptic transfer for this viral vector[39]. In the PVH, some POMC axon projections expressed tdtomato, and PVH somata postsynaptic to POMC neurons were identified by tdtomato expression (Supplementary Fig. 6c). Many of these labeled PVH somata overlapped with clusters of AGRP-immunoreactive boutons (Supplementary Fig. 6d–h). Although some of these boutons may be non-synaptic or onto adjacent dendrites, based on our EM analysis, a substantial fraction is predicted to be somatic (on average 26%, Fig. 6a). In support of this, inspection of our EM data did not show evidence of PVH somata contacted by an AGRP neuron synapse within one bouton-length of each other as an alternative somatic target. Therefore, convergent synaptic connections of AGRP and POMC axon projections onto the same neurons in the PVH are indicated for the tdtomato-labeled PVH somata with larger numbers of juxtaposed AGRP boutons (Supplementary Fig. 6i,j).

DISCUSSION

Neural circuit connectivity between molecularly defined cell types provides an important framework for examining brain function. Our results demonstrate that GESEM-labeling of synaptic vesicles by VAMP2:HRP enables high-resolution, cell type-specific ultrastructure in mouse brains and is also compatible with fly brains. This technique for identifying synapses from molecularly defined neurons is an alternative to technically difficult immuno-EM approaches, and it is readily implemented to label the axon projections of Cre-expressing or GAL4-expressing cell types. This approach enabled us to perform high quality serial section reconstruction of genetically labeled axon projections, which was essential here for quantitative analysis of cell type-specific connectivity and could not be readily

achieved with prior functional and anatomical approaches[36,40]. In addition, GESEM-labeling facilitates visualization of cell type-specific circuit communication channels embedded in the context of other circuit interactions as well as sub-synaptic, cell biological characteristics of these interactions. Long-range ultrastructure mapping is thus an information-rich method that complements existing functional[6,7] and viral tracing[5, 39, 41] circuit mapping techniques.

Technical considerations for GESEM labeling

This method for cell type-specific ultrastructural circuit mapping is based on viral expression of vesicle-targeted HRP as a synaptic marker. This release site labeling strategy offers several useful characteristics. (1) Genetic expression of an EM contrast generator allowed reproducible labeling of synapses from molecularly defined cell types. (2) Because the marker is already present at the synapse when the tissue is prepared for imaging, there is no need for antibody labeling. (3) Due to ubiquitous expression of VAMP2 in vesicular structures[28], HRP can label terminals that may not be detectable with immunolabeling against a cell type-specific marker. For example, we found that some POMC terminals have few or no LVs (Fig. 5a), which would make them undetectable by immunoreactivity to an anti-POMC antibody[40,42]. In addition, carboxy-terminal tagging of VAMP2 has been used extensively for intravesicular protein targeting and does not interfere with vesicle fusion[43]. (4) HRP is not functional in the cytoplasm[18] therefore previous attempts to express a soluble version have been ineffective. Genetically encoded labeling by extracellularly targeted HRP can obscure structures that are critical for determination of connectivity[14]. On the other hand, vesicular labeling can be readily detected and does not obscure intracellular and extracellular compartments since the DAB oxidation precipitate is trapped within the vesicles. (5) DAB precipitate entrapment in the compact vesicle volume also acts as a natural contrast enhancer, eliminating the extra step of tyramide signal amplification enhancement, which is required for a membrane targeted variant because of its sparse distribution[14]. Avoiding this extra enhancement step in our method further minimized perturbation to ultrastructure.

Not all vesicles were labeled by the DAB reaction (Fig. 1d,e and Fig. 4). Similar incomplete labeling was previously reported for VAMP2:HRP in cultured neurons[27]. According to an estimate from artificial liposomes (60 – 80 nm diameter), a single HRP molecule is sufficient to fill the vesicle lumen with DAB reaction product[44]. Therefore, the lack of labeling may indicate the absence of functional VAMP2:HRP chimera from these vesicles. However, VAMP2 is one of the most abundant proteins in the vesicle membrane (~70 copies/vesicle)[45]. Because VAMP2:HRP was expressed for more than 3 weeks under a strong promoter, we expected that most vesicles would contain at least a single copy of the chimera in our samples. It is possible that vesicles already in use before viral transduction may not readily accept new VAMP2 molecules, but extensive vesicular protein intermixing has been reported in hippocampal cultures[46]. Therefore this scenario seem unlikely, although we cannot rule out the possibility that intermixing in a distal projection might require a longer time. In addition, it is also possible that our fixation and labeling conditions might reduce the efficiency of HRP oxidation of DAB or inactivate a portion of the HRP molecules. Nevertheless, since only a few electron-dense, DAB-labeled vesicles are

sufficient for identification, even with partial vesicle labeling penetrance, the GESEM method is effective for cell type-specific labeling. The variable efficacy of labeling due to viral transduction levels could be overcome by selecting only the highest efficiency viral injections for analysis. Alternatively, generation of a Cre-dependent VAMP2:HRP reporter mouse line would facilitate high-penetrance GESEM labeling.

We also observed boutons with electron-dense DAB reaction product on the extracellular portion of the plasma membrane of GESEM-labeled boutons (Supplementary Fig. 3). This labeling indicates extracellularly directed HRP, which is the orientation expected of the VAMP2:HRP chimeric protein after vesicle exocytosis. Therefore, extracellular labeling may be associated with recent synaptic vesicle fusion. The possibility that VAMP2:HRP could report recent synaptic activity in the context of ultrastructure circuit mapping could be developed to provide an additional level of insight into circuit function.

Synaptic organization of a feeding circuit

Energy sensing AGRP and POMC neuron populations function in an antagonistic fashion to regulate feeding behavior. The interaction of these neurons involves axon projections to the PVH and reciprocal regulation of PVH neuron melanocortin receptors by release of the agonist, α-melanocyte stimulating hormone from POMC neurons, and the corresponding inverse agonist, AGRP from AGRP neurons[25,47]. Optogenetic and chemogenetic experiments in POMC and AGRP neurons suggest that the melanocortin pathway influences food consumption over a timescale of hours to days[22,24,48]. However, recent work on the $ARC^{AGRP}\rightarrow PVH$ circuit in behaving mice has emphasized key roles for NPY and GABA to induce food seeking and consumption within minutes through a melanocortin receptor-independent pathway[24,48]. This observation indicated a more complex circuit than was evident in models focused solely on regulation of melanocortin receptor signaling.

Consistent with the prominent role for both neuropeptide and fast amino acid neurotransmission in these circuits, we observed that GESEM-labeled boutons showed vesicle profiles that typically had a mix of SVs and LVs, ranging from predominantly SV-containing synaptic connections to LV-only boutons (Fig. 5a). Overall, non-synaptic boutons for both cell types had abundant LVs and often had fewer SVs than boutons with a synaptic contact. The non-synaptic AGRP and POMC neuron boutons that we imaged have features similar to non-synaptic release sites for other neuromodulators and neuropeptides[30]. $ARC^{AGRP}\rightarrow PVH$ projections showed a greater proportion of non-synaptic boutons, and some of these showed electron-dense DAB reaction product on the extracellular membrane (Supplementary Fig. 3a,b). This is indicative of synaptic vesicle exocytosis and is evidence that these non-synaptic boutons are LV release sites. Furthermore, we observed several putative Ω-structures in non-synaptic boutons (Supplementary Fig. 3c–h), which can be due to recent vesicle fusion events[32]. Taken together, EM analysis of GESEM-labeled non-synaptic $ARC^{AGRP}\rightarrow PVH$ boutons indicates that some are likely release sites for their LV contents (presumably peptidergic). Interestingly, for $ARC^{AGRP}\rightarrow PVH$ axons in which multiple connected boutons were reconstructed in the volume imaged by EM, many (9/11) showed examples of SV-rich synaptic contacts adjacent to predominantly LV-containing non-synaptic boutons. Although this observation is from a limited PVH volume from a

single mouse, it indicates that the same ARC^{AGRP}→PVH axons can contain two types of boutons that are either predominantly peptidergic or combined neurotransmitter/peptide release sites.

In these molecularly defined circuits, we also observed differential distribution of mitochondria between synaptic and non-synaptic boutons, irrespective of the cell type analyzed. In light of the multifaceted functional roles of mitochondria, these observations might indicate potential differences in the energetic regulation and calcium handling within distinct, specialized release sites that mediate non-synaptic peptidergic transmission and synaptic fast neurotransmitter/peptidergic co-transmission. One possible functional implication is that, because LV fusion is regulated by a cumulative rise in intra-terminal calcium[49], this configuration may facilitate neuropeptide release at lower electrical activity levels from the subset of release sites lacking mitochondria, which are typically non-synaptic. Given the necessity of neuropeptide release for AGRP neuron evoked feeding[24], the presence of peptidergic release sites tuned to different activity levels would be consistent with the observation of evoked food intake even at low AGRP neuron firing frequencies[22].

Our initial observations of GESEM-labeled boutons indicate that the structure of these circuits is more specialized than expected from a model focused solely on antagonistic peptidergic regulation of melanocortin receptor signaling. In PVH neurons, dendrites are targeted by predominantly excitatory POMC neuron synapses (Fig. 6a) and synapses from other cell types. As in other circuits[50], distal synaptic input is likely insufficient to drive neuronal excitation and would require coincident activity from other dendritic inputs. In support of this, the identified excitatory POMC synapses had small PSD areas and synaptic current amplitudes. On the other hand, the somato-centric, multi-synapse ARC^{AGRP}→PVH connections, in combination with the asynchronous release property of these synapses[24], mediate strong PVH neuron inhibition[24]. Therefore, these two circuits appear to target different PVH neuronal compartments and are not configured as directly opposing interactions. However, because these ultra-structural data were obtained from a single animal for each experiment (AGRP or POMC), a larger sample size (and, ideally, larger volume reconstructions) will be needed to draw robust conclusions about the organization of the ARC→PVH circuitry. Furthermore, transsynaptic viral tracing experiments (Supplementary Fig. 6), indicated that some PVH neurons receive convergent input from both cell types. Based on these data, we speculate that the synaptic arrangement found here is consistent with a circuit in which distal inputs, including from POMC neurons, are summed to influence PVH neuron activity, and this can be vetoed by long-range somatic AGRP neuron input. In agreement with this, experiments that simultaneously co-activate AGRP and POMC neurons result in voracious eating similar to activating AGRP neurons alone[24], and direct suppression of PVH activity elicits intense food intake[24]. Therefore, ultrastructural analysis shows a circuit configuration that favors feeding behavior under conditions of elevated AGRP neuron activity.

Conclusions

GESEM-labeling enables long-range, high resolution mapping of cell type-specific connections in complex molecularly defined neural circuits. Because this approach allows

excellent preservation of ultrastructure, it facilitates reconstruction of molecularly defined axon segments as well as systematic and quantitative analysis of their axonal boutons and synapses. Future refinement of this method could involve combination with EM markers targeted to different subcellular compartments[13-16,19] to enable simultaneous labeling of pre- and post-synaptic neuronal cell types. In concert with functional circuit mapping techniques, GESEM-labeling could be a powerful tool for achieving cell type-specific connectomes.

Methods

All experimental protocols were conducted according to U.S. National Institutes of Health guidelines for animal research and were approved by the Institutional Animal Care and Use Committee at Janelia Farm Research Campus.

Mice

Agrp-Cre[51], *Pomc-Cre*[52] male mice were used for GESEM ultrastructural analysis. Other mice used were *Agrp-IRES-Cre*[53];*Ai9* (*ROSA-loxPStoploxP-tdTomato*)[54], and *POMC-topazFP*[55]. Background strains of mice were C57Bl6 or C57Bl6/FVB hybrid. Mice were given *ad libitum* access to food and were housed in a 12 h:12 h light-dark cycle, with lights on at 6:00 a.m. Prior to viral injection surgery, mice were housed in cages in groups ≤5. Following surgery, mice were singly housed.

Stereotactic rAAV and HSV injections

Vamp2:HRP was obtained by removing the stop codon in the *Vamp-2* coding sequence (*Bos taurus*, aa 1 – 115) and ligating the HRP cDNA at the 3′ end. Between the two cDNAs is a sequence encoding a linker peptide (TAGGSGGTGGSGGT) and a 2× Myc-tag polypeptide sequence (EQKLISEEDLEEQKLISEEDL). The cDNA encoding the chimeric protein was then inserted into rAAV2-*CAG-FLEX* backbone in the inverted orientation to create the Cre-dependent viral expression vector (serotype 1), rAAV2-*CAG-FLEX-rev-Vamp2:HRP* (construct available from http://www.addgene.org/Scott_Sternson/). Viral injections were performed as described previously[7]. ARC coordinates: bregma −1.2 mm, midline ±0.2 mm; dorsal surface −5.85 mm and −5.75 mm, total of 600 nL of virus injected per side. rAAV2/1-*CAG-FLEX-rev-Vamp2:HRP*, was produced by the University of Pennsylvania Gene Therapy Program Vector Core (titer: 3e13 GC/mL). Mice were injected with the viral vector between P21 - P25.

For circuit mapping experiments, rAAV2/1-CAG-*FLEX-rev-ChR2:tdtomato* was used as described previously[7]. For HSV injections, HSV129-loxP-STOP-loxP-*tdtomato:2a:TK* (H129ΔTK-TT, was obtained from the Center for Neuroanatomy with Neurotropic Viruses, strain H356). Viral injections (100 nL at each site) were made with BSL2 precautions into ARC coordinates (medial/lateral: 0.25 mm; anterior/posterior: −1.4 mm; dorsal/ventral: −5.9 mm, −5.8 mm, −5.7 mm). Viral titer was 1.3e9 pfu/mL. After a short incubation time (~36 h, which is associated with anterograde transfer across one synapse[39]), in BSL2 housing, mice were perfused and processed for immunohistochemistry (see below). Tdtomato expression was Cre-dependent, as injection of the H129ΔTK-TT viral vector into C57BL6 mice lacking Cre-recombinase did not show tdtomato expression.

Electron microscopy

AGRP and POMC neurons in the ARC of three week old *Agrp-Cre* and *Pomc-Cre* mice were transduced with a Cre-dependent virus expressing VAMP2:HRP (rAAV2/1-*CAG-FLEX-rev-Vamp2:HRP*). Four weeks post-infection animals were transcardially perfused during the light period with 4% paraformaldehyde and 0.8% glutaraldehyde in 0.1 M phosphate buffer. Brain tissue was vibratome sectioned (100 μm) in 0.1 M Na-cacodylate buffer and processed for electron microscopy at room temperature. We injected several mice and used only the best transduced brains for EM processing. For this, we screened brain sections for viral transduction using Tyramide-FITC or tyramide-Cy3 treatment (TSA™; Perkin-Elmer). HRP derived fluorescence signal is monitored in the PVH area of slices, and the adjacent untreated vibratome sections were selected for processing for large-scale EM imaging. The brain slices were rinsed 2 × 10 minutes with 50 mM glycine in 0.1 M Na-cacodylate buffer followed by 0.1 M Na-cacodylate buffer containing 0.1% saponin 2 × 15 minutes to increase membrane permeability without compromising membrane ultrastructure[56]. The brain slices were then incubated in 1 ml of 3,3′-diaminobenzidine tetrahydrochloride (DAB) (Sigma Chemical Co., cat. no. D5905-50TAB) at 0.3 mg/mL in 0.1 M Na-cacodylate/0.1% saponin buffer for 30 minutes in the dark. The DAB reaction was initiated by the addition of 10 μL 0.003% H_2O_2 and allowed to proceed for 1.5 h in the dark. The samples were rinsed with 0.1 M Na-cacodylate buffer, and then post-fixed with 1% reduced[57] OsO_4 in 0.1 M Na-cacodylate for 30 min. The samples were then rinsed in distilled water, dehydrated in ethanol followed by propylene oxide and embedded in Eponate 12 resin (Ted Pella, Inc.).

Brains from 7 day adult w^{1118} [iso] 5905 × [iso] Canton S G1 flies were isolated by dissection in cold saline and fixed for 1 hour in 1% glutaraldehyde in 0.1 M Na-cacodylate buffer on ice. Subsequent processing steps beginning with rinses in 0.1 M Na-cacodylate buffer containing 50 mM glycine were identical to those for HRP staining of mouse brain tissue.

Ultrathin serial 60 nm sections were cut with a Diatome diamond knife using a Leica UC6 ultramicrotome and picked up on Pioloform films on slot grids. Sections on grids were stained with 1% uranyl acetate followed by lead citrate. Sections were examined and photographed using an FEI Spirit BioTWIN TEM equipped with a Gatan U895 4k camera (3.8 nm/pixel) using the Leginon automated imaging software[58], resulting in a mosaic of overlapping images for each section. Images were assembled using Fiji with fine alignment using Raveler software as described elsewhere[59]. Briefly, alignment points, both within overlapping images and between adjacent sections, were found by cross-correlation of image patches. A least-squares fit then generated an affine transformation per image, mapping it into a global solution. Remaining discontinuities, caused by lens distortion and other non-linearities, were minimized by defining 21 control points for each image, which were adjusted by least-squares fit to bring corresponding features into alignment, resulting in a single large flat image per section.

Within each of these assembled images, DAB reaction product-labeled features were identified manually and selected for analysis. Synapses were modeled with Fiji/

TrakEM2[60,61]. The first 51 complete boutons identified from each sample were used for SV, LV, and mitochondria quantification (**Figs. 5a-h**). To check for possible artifactual differences that could be caused by slight differences in region selection from different mice or sample preparation and imaging, investigators blind to sample identity compared the same anatomical parameters taken from the unlabeled parts of same images. Unlike for the labeled boutons and their targets, we did not observe significant differences in several parameters [number of SVs, *Agrp-Cre* control boutons: 463 ± 53, *Pomc-Cre* control boutons: 631 ± 75; number of LVs: *Agrp-Cre* control boutons: 22 ± 3, *Pomc-Cre* control boutons: 21 ± 3; number of synaptic mitochondria, *Agrp-Cre* control boutons: 1.7 ± 0.25, *Pomc-Cre* control boutons: 1.9 ± 0.2; dendritic diameter, *Agrp-Cre* control boutons: 1.6 ± 0.07 μm, *Pomc-Cre* control boutons: 1.7 ± 0.08 μm (n = 34 unlabeled boutons nearby labeled AGRP boutons from one *Agrp-Cre* mouse and n = 41 unlabeled boutons nearby labeled POMC boutons from one *Pomc-Cre* mouse, $P > 0.05$ in all comparisons between control bouton measurements from *Agrp-Cre* and *Pomc-Cre* mouse data sets)].

Axonal bouton and synapse classification

An axonal segment was classified as a bouton if it contained clustered vesicles and its diameter was >3 times neighboring axonal segments (typically 200 – 400 nm in width). For a bouton to be classified as having synaptic contact, we used two criteria: 1) parallel pre- and post-synaptic membranes (extending >200 nm), 2) clustered SVs in contact with this membrane. Some boutons were completely reconstructed within the imaged volume but did not have an identifiable postsynaptic partner. Another group of boutons were partially reconstructed and had a clear identifiable postsynaptic partner. For classification of boutons as symmetric and asymmetric, we examined the entire bouton for presence of a postsynaptic density (an electron dense protrusion into the postsynaptic cytosol) and focused on the sections that contained docked vesicles. In cases with two synaptic contacts from the same axon, each showed the same morphology ($ARC^{AGRP}\rightarrow$PVH: 1 axon, both synapses symmetric; $ARC^{POMC}\rightarrow$PVH: 4 axons, all synapses asymmetric; 1 axon, both synapses symmetric). A subset of synapses were classified as *en face* if they had clustered SVs near contact sites, but the synaptic cleft was obscured because the tissue sectioning angle was in the plane of the contact site. For some boutons, missing sections or a damaged membrane did not allow clear determination of synaptic or non-synaptic type, and they were classified as undetermined.

Electrophysiology

Experimental techniques were similar to those reported previously[7], and only the differences are described here. After viral infection (10 – 14 days incubation) mice were deeply anaesthetized with isoflurane and decapitated. Coronal brain slices containing the PVH (300 μm) were prepared in chilled cutting solution containing (in mM): 234 sucrose, 28 $NaHCO_3$, 7 dextrose, 2.5 KCl, 7 $MgCl_2$, 0.5 $CaCl_2$, 1 sodium ascorbate, 3 sodium pyruvate and 1.25 mM NaH_2PO_4, aerated with 95% O_2/5% CO_2. Slices were transferred to artificial cerebrospinal fluid (aCSF) containing (in mM): 119 NaCl, 25 $NaHCO_3$, 11 D-glucose, 2.5 KCl, 1.25 $MgCl_2$, 2 $CaCl_2$ and 1.25 NaH_2PO_4, aerated with 95% O_2/5% CO_2. Slices were incubated at 34 °C for 30 minutes and then maintained and recorded from at room temperature (20– 24 °C). Axons were identified and targeted by tdtomato fluorescence

emission. Neurons were patched using electrodes with tip resistances 4 – 5 MΩ. The intracellular solution for voltage clamp recordings contained (in mM): 125 CsCl, 5 NaCl, 10 HEPES, 0.6 EGTA, 4 Mg-ATP, 0.3 Na_2GTP, 10 lidocaine *N*-ethyl bromide (QX-314), pH 7.35 and 290 mOsm. The holding potential for voltage clamp recordings was −60 mV. In most recordings, internal GTP was replaced by GDP-βS (0.5 mM, Sigma).

Photostimulation

A laser (473 nm, CrystaLaser) was used to deliver photostimuli ranging from 0.01 – 1 mW. Neutral density filters were used to control the laser power at the specimen. Light pulse duration (1 ms) was controlled by a Pockels cell (ConOptics) and a mechanical shutter (Vincent Associates). A focal spot was targeted onto the specimen with two x–y scanning mirrors (Cambridge Technology) through a 4× or a 63× objective (Olympus). Laser power was monitored with a photodiode for each light pulse.

Evoked $ARC^{AGRP}\rightarrow$PVH quantal amplitude measurements were performed under the same conditions as above except that, in the aCSF, Ca^{2+} (2 mM) was replaced by Sr^{2+} (2 mM). Quantal events were chosen from a window immediately following stimulation until the event frequency dropped to three times above the baseline spontaneous event frequency.

For minimal stimulation, whole cell voltage clamp was established and synaptic connectivity was tested using maximal laser intensity. Afterwards, the light intensity was reduced progressively using a neutral density filter, while monitoring synaptic release until photostimulation failed to induce synaptic release in >50% of the trials for at least 20 consecutive trials. Additional photostimulation trials were typically obtained.

Pharmacology

Drugs were bath applied with a gravity perfusion system. Blockers and final concentrations were as follows: glutamate receptors (AP-5, 50 μM; CNQX, 10 μM) and $GABA_A$ receptors were blocked (picrotoxin, 50 μM; Sigma). In initial POMC and AGRP connectivity recordings, first measurements are performed in the absence of blockers, then sequentially AP-5 and CNQX or picrotoxin added to confirm nature of connection. In all other measurements with AGRP connections, saclofen (50 μM, Tocris), AP-5 and CNQX were used. Saclofen was included to prevent metabotropic GABA-mediated modulation of the postsynaptic neuron.

Antibodies

Rabbit anti-NPY[62] (1:2000, ImmunoStar 22940), Goat anti-AGRP (1:5000, Neuromics GT15023)[63], guinea pig anti-RFP[24] (1:25000, Covance), rabbit anti-POMC (27–52)[55] (1:2000 Phoenix Pharmaceuticals, H02930), rabbit anti-GFP (1:5000, Invitrogen A-11122), sheep anti-GFP (1:3000, AbD Serotec 47451051), rabbit anti-vGlut1[64] (1:2000, SYSY, 135302), guinea pig anti-vGlut2 (1:2000, SYSY 135404), rabbit anti-vGlut2[65] (1:1000, SYSY 135402), mouse anti-vGat (1:100, SYSY 131011), rabbit anti-vGat[66] (1:4000, Covance), goat anti-vAcht (1:2000, Chemicon ABN100). Fluorophore-conjugated, minimal cross reactivity secondary antibodies were from Jackson Immuno (1:500).

Immunohistochemistry and imaging

Mice were perfused with 4% paraformaldehyde in 0.1 M phosphate buffer fixative (pH 7.4). Tissue was post-fixed in this solution for 3 – 4 h and washed overnight in phosphate buffered saline (PBS) (pH 7.4). Brain slices (20 – 200 μm thick, for imaging in the first 10 μm from the surface) were incubated overnight at 4° C with primary antibodies diluted in PBS, supplemented with 1% BSA and 0.1% Triton X-100. Slices were then washed 3 times and incubated with species appropriate and minimally cross reactive fluorophore-conjugated secondary antibodies for 2 hours at room temperature. Slices were rinsed in PBS (2 times) and mounted for imaging using hardset Vectashield (H-1400).

PVH boutons were imaged with a Zeiss LSM 510 using a 63× objective, NA: 1.4 to obtain confocal images with a z-section of less than 0.9 μm per image for excitation with 488 nm, 561 nm, and 633nm laser lines. Confocal stacks of 10 – 15 sections were obtained to facilitate complete reconstruction of individual AGRP or POMC boutons.

Colocalization analysis

For examination of molecular characteristics of AGRP boutons, *Agrp-IRES-Cre* mice were crossed with *Ai9* (*ROSA-loxPSTOPloxP-tdtomato*) mice. POMC boutons were identified in *Pomc-topazFP* transgenic mice[55]. We performed colocalization analysis by first using fluorescence from tdtomato or topazFP to identify AGRP and POMC boutons respectively, without regard to the presence of other synaptic markers. We also determined that the complete bouton was captured in our image stack. This subset of boutons was then assessed for the presence of peptidergic and neurotransmitter transporters (AGRP, NPY, vGat, vGlut1, vGlut2, and vAcht).

Fluorescence image analysis of transsynaptically labeled PVH neurons

Images were obtained from 10 sections, 2 mice (5 from each mouse) and were collected with a Zeiss LSM 510 microscope using a 63× objective, NA: 1.4. The fluorescence signal acquired for each channel was maintained in the linear range, the pinhole was constrained to less than or equal to 1 airy unit (AU]), and sampling in the z-axis was performed at 0.5× the optical resolution of the objective. To identify AGRP boutons on transsynaptically labeled (tdtomato-expressing) PVH neurons, images were obtained in the PVH containing complete neuronal somata of tdtomato-labeled neurons in the X, Y, and Z axes. Juxtaposed AGRP boutons with tdtomato-labeled PVH somata and proximal dendrites were identified by analyzing the images in the XY, XZ, and YZ planes. Only AGRP boutons that overlapped or contacted tdtomato labeling in all three axes were scored as contacts.

Statistics

Values are represented as mean ± s.e.m. P-values for pair-wise comparisons were calculated using Microsoft Excel and SigmaPlot by Mann-Whitney U-test (because conditions of equal variance were violated). For **Fig. 5l**, we used two-tailed paired Student's t-tests, for which the normality condition was satisfied based on the Shapiro-Wilk test. No statistical methods were used to predetermine sample sizes, but our sample sizes are similar to those employed in the field[8,37]. Sample sizes of 51 boutons reflected the first manually identified 51

boutons, which were chosen as the subset to be used for detailed quantitative analysis. Sampling was semi-random as it reflected the order of identification of the labeled boutons and no specific feature of the labeled boutons. In the case of identification of boutons connected by an axonal segment, these were found by analyzing the entire sample of labeled boutons identified in the imaged volume. n.s. $P > 0.05$, $*P < 0.05$, $**P < 0.01$, $***P < 0.001$. A supplementary methods checklist is available.

Supplementary Material

Refer to Web version on PubMed Central for supplementary material.

Acknowledgements

This research was funded by the Howard Hughes Medical Institute. HSV129ΔTK-TT anterograde transsynaptic tracer virus was from the Center for Neuroanatomy with Neurotropic Viruses (P40RR018604). We thank A. Wardlaw for mouse breeding and genotyping; K. Morris for HSV stereotaxic injections; A. Hu and M. Copeland for histology; L. Lo, D. Anderson, and R. Gong with advice on HSV129 anterograde tracing

REFERENCES

1. Luo L, Callaway EM, Svoboda K. Genetic dissection of neural circuits. Neuron. 2008; 57:634–660. [PubMed: 18341986]
2. Mishchenko Y, et al. Ultrastructural analysis of hippocampal neuropil from the connectomics perspective. Neuron. 2010; 67:1009–1020. [PubMed: 20869597]
3. Dani A, Huang B, Bergan J, Dulac C, Zhuang X. Superresolution imaging of chemical synapses in the brain. Neuron. 2010; 68:843–856. [PubMed: 21144999]
4. Feinberg EH, et al. GFP Reconstitution Across Synaptic Partners (GRASP) defines cell contacts and synapses in living nervous systems. Neuron. 2008; 57:353–363. [PubMed: 18255029]
5. Wall NR, Wickersham IR, Cetin A, De La Parra M, Callaway EM. Monosynaptic circuit tracing in vivo through Cre-dependent targeting and complementation of modified rabies virus. Proc. Natl. Acad. Sci. U. S. A. 2010; 107:21848–21853. [PubMed: 21115815]
6. Petreanu L, Huber D, Sobczyk A, Svoboda K. Channelrhodopsin-2-assisted circuit mapping of long-range callosal projections. Nat. Neurosci. 2007; 10:663–668. [PubMed: 17435752]
7. Atasoy D, Aponte Y, Su HH, Sternson SM. A FLEX switch targets Channelrhodopsin-2 to multiple cell types for imaging and long-range circuit mapping. J. Neurosci. 2008; 28:7025–7030. [PubMed: 18614669]
8. Bock DD, et al. Network anatomy and in vivo physiology of visual cortical neurons. Nature. 2011; 471:177–182. [PubMed: 21390124]
9. Briggman KL, Helmstaedter M, Denk W. Wiring specificity in the direction-selectivity circuit of the retina. Nature. 2011; 471:183–188. [PubMed: 21390125]
10. Takemura SY, et al. A visual motion detection circuit suggested by Drosophila connectomics. Nature. 2013; 500:175–181. [PubMed: 23925240]
11. Knott GW, Holtmaat A, Trachtenberg JT, Svoboda K, Welker E. A protocol for preparing GFP-labeled neurons previously imaged in vivo and in slice preparations for light and electron microscopic analysis. Nat Protoc. 2009; 4:1145–1156. [PubMed: 19617886]
12. Gustincich S, Feigenspan A, Wu DK, Koopman LJ, Raviola E. Control of dopamine release in the retina: a transgenic approach to neural networks. Neuron. 1997; 18:723–736. [PubMed: 9182798]
13. Dubois L, Lecourtois M, Alexandre C, Hirst E, Vincent JP. Regulated endocytic routing modulates wingless signaling in Drosophila embryos. Cell. 2001; 105:613–624. [PubMed: 11389831]
14. Li J, Wang Y, Chiu S-L, Cline H. Membrane targeted horseradish peroxidase as a marker for correlative fluorescence and electron microscopy studies. Frontiers in Neural Circuits. 2010; 4

15. Shu X, et al. A genetically encoded tag for correlated light and electron microscopy of intact cells, tissues, and organisms. PLoS Biol. 2011; 9:e1001041. [PubMed: 21483721]
16. Martell JD, et al. Engineered ascorbate peroxidase as a genetically encoded reporter for electron microscopy. Nat. Biotechnol. 2012; 30:1143–1148. [PubMed: 23086203]
17. Watts RJ, Schuldiner O, Perrino J, Larsen C, Luo L. Glia engulf degenerating axons during developmental axon pruning. Curr. Biol. 2004; 14:678–684. [PubMed: 15084282]
18. Hopkins C, Gibson A, Stinchcombe J, Futter C. Chimeric molecules employing horseradish peroxidase as reporter enzyme for protein localization in the electron microscope. Methods Enzymol. 2000; 327:35–45. [PubMed: 11044972]
19. Schikorski T, Young SM Jr. Hu Y. Horseradish peroxidase cDNA as a marker for electron microscopy in neurons. J. Neurosci. Methods. 2007; 165:210–215. [PubMed: 17631969]
20. Bozzola, JJ.; Russell, LD. Electron microscopy. Principles and Techniques for Biologists. 2nd edn. Jones and Bartlett Publishers; 1999.
21. Gao Q, Horvath TL. Neurobiology of feeding and energy expenditure. Annu. Rev. Neurosci. 2007; 30:367–398. [PubMed: 17506645]
22. Aponte Y, Atasoy D, Sternson SM. AGRP neurons are sufficient to orchestrate feeding behavior rapidly and without training. Nat. Neurosci. 2011; 14:351–355. [PubMed: 21209617]
23. Krashes MJ, et al. Rapid, reversible activation of AgRP neurons drives feeding behavior in mice. J Clin Invest. 2011; 121:1424–1428. [PubMed: 21364278]
24. Atasoy D, Betley JN, Su HH, Sternson SM. Deconstruction of a neural circuit for hunger. Nature. 2012; 488:172–177. [PubMed: 22801496]
25. Balthasar N, et al. Divergence of melanocortin pathways in the control of food intake and energy expenditure. Cell. 2005; 123:493–505. [PubMed: 16269339]
26. Diano S, Naftolin F, Goglia F, Csernus V, Horvath TL. Monosynaptic pathway between the arcuate nucleus expressing glial type II iodothyronine 5′-deiodinase mRNA and the median eminence-projective TRH cells of the rat paraventricular nucleus. J. Neuroendocrinol. 1998; 10:731–742. [PubMed: 9792325]
27. Leal-Ortiz S, et al. Piccolo modulation of Synapsin1a dynamics regulates synaptic vesicle exocytosis. J. Cell Biol. 2008; 181:831–846. [PubMed: 18519737]
28. Li JY, Edelmann L, Jahn R, Dahlstrom A. Axonal transport and distribution of synaptobrevin I and II in the rat peripheral nervous system. J. Neurosci. 1996; 16:137–147. [PubMed: 8613780]
29. Cowley MA, et al. Leptin activates anorexigenic POMC neurons through a neural network in the arcuate nucleus. Nature. 2001; 411:480–484. [PubMed: 11373681]
30. Buma P. Characterization of luteinizing hormone-releasing hormone fibres in the mesencephalic central grey substance of the rat. Neuroendocrinology. 1989; 49:623–630. [PubMed: 2475815]
31. Schikorski T, Stevens CF. Morphological correlates of functionally defined synaptic vesicle populations. Nat. Neurosci. 2001; 4:391–395. [PubMed: 11276229]
32. Buma P, Roubos EW. Ultrastructural demonstration of nonsynaptic release sites in the central nervous system of the snail Lymnaea stagnalis, the insect Periplaneta americana, and the rat. Neuroscience. 1986; 17:867–879. [PubMed: 3703256]
33. Vos M, Lauwers E, Verstreken P. Synaptic mitochondria in synaptic transmission and organization of vesicle pools in health and disease. Front Synaptic Neurosci. 2010; 2:139. [PubMed: 21423525]
34. Williams SR, Stuart GJ. Role of dendritic synapse location in the control of action potential output. Trends Neurosci. 2003; 26:147–154. [PubMed: 12591217]
35. van den Pol AN. The magnocellular and parvocellular paraventricular nucleus of rat: intrinsic organization. J. Comp. Neurol. 1982; 206:317–345. [PubMed: 7096631]
36. Legradi G, Lechan RM. Agouti-related protein containing nerve terminals innervate thyrotropin-releasing hormone neurons in the hypothalamic paraventricular nucleus. Endocrinology. 1999; 140:3643–3652. [PubMed: 10433222]
37. Harris KM, Stevens JK. Dendritic spines of CA 1 pyramidal cells in the rat hippocampus: serial electron microscopy with reference to their biophysical characteristics. J. Neurosci. 1989; 9:2982–2997. [PubMed: 2769375]

38. Cruikshank SJ, Urabe H, Nurmikko AV, Connors BW. Pathway-specific feedforward circuits between thalamus and neocortex revealed by selective optical stimulation of axons. Neuron. 2010; 65:230–245. [PubMed: 20152129]
39. Lo L, Anderson DJ. A Cre-dependent, anterograde transsynaptic viral tracer for mapping output pathways of genetically marked neurons. Neuron. 2011; 72:938–950. [PubMed: 22196330]
40. Liposits Z, Sievers L, Paull WK. Neuropeptide-Y and ACTH-immunoreactive innervation of corticotropin releasing factor (CRF)-synthesizing neurons in the hypothalamus of the rat. An immunocytochemical analysis at the light and electron microscopic levels. Histochemistry. 1988; 88:227–234. [PubMed: 2835333]
41. Beier KT, et al. Anterograde or retrograde transsynaptic labeling of CNS neurons with vesicular stomatitis virus vectors. Proc. Natl. Acad. Sci. U. S. A. 2011; 108:15414–15419. [PubMed: 21825165]
42. Fekete C, et al. alpha-Melanocyte-stimulating hormone is contained in nerve terminals innervating thyrotropin-releasing hormone-synthesizing neurons in the hypothalamic paraventricular nucleus and prevents fasting-induced suppression of prothyrotropin-releasing hormone gene expression. J. Neurosci. 2000; 20:1550–1558. [PubMed: 10662844]
43. Miesenbock G, De Angelis DA, Rothman JE. Visualizing secretion and synaptic transmission with pH-sensitive green fluorescent proteins. Nature. 1998; 394:192–195. [PubMed: 9671304]
44. Stinchcombe JC, Nomoto H, Cutler DF, Hopkins CR. Anterograde and retrograde traffic between the rough endoplasmic reticulum and the Golgi complex. J. Cell Biol. 1995; 131:1387–1401. [PubMed: 8522599]
45. Takamori S, et al. Molecular anatomy of a trafficking organelle. Cell. 2006; 127:831–846. [PubMed: 17110340]
46. Fernandez-Alfonso T, Kwan R, Ryan TA. Synaptic vesicles interchange their membrane proteins with a large surface reservoir during recycling. Neuron. 2006; 51:179–186. [PubMed: 16846853]
47. Fan W, Boston BA, Kesterson RA, Hruby VJ, Cone RD. Role of melanocortinergic neurons in feeding and the agouti obesity syndrome. Nature. 1997; 385:165–168. [PubMed: 8990120]
48. Krashes MJ, Shah BP, Koda S, Lowell BB. Rapid versus Delayed Stimulation of Feeding by the Endogenously Released AgRP Neuron Mediators GABA, NPY, and AgRP. Cell Metab. 2013; 18:588–595. [PubMed: 24093681]
49. Peng YY, Zucker RS. Release of LHRH is linearly related to the time integral of presynaptic Ca2+ elevation above a threshold level in bullfrog sympathetic ganglia. Neuron. 1993; 10:465–473. [PubMed: 8461136]
50. Xu NL, et al. Nonlinear dendritic integration of sensory and motor input during an active sensing task. Nature. 2012; 492:247–251. [PubMed: 23143335]
51. Kaelin CB, Xu AW, Lu XY, Barsh GS. Transcriptional regulation of agouti-related protein (Agrp) in transgenic mice. Endocrinology. 2004; 145:5798–5806. [PubMed: 15345681]
52. Balthasar N, et al. Leptin receptor signaling in POMC neurons is required for normal body weight homeostasis. Neuron. 2004; 42:983–991. [PubMed: 15207242]
53. Tong Q, Ye CP, Jones JE, Elmquist JK, Lowell BB. Synaptic release of GABA by AgRP neurons is required for normal regulation of energy balance. Nature Neurosci. 2008; 11:998–1000. [PubMed: 19160495]
54. Madisen L, et al. A robust and high-throughput Cre reporting and characterization system for the whole mouse brain. Nat. Neurosci. 2010; 13:133–140. [PubMed: 20023653]
55. Pinto S, et al. Rapid rewiring of arcuate nucleus feeding circuits by leptin. Science. 2004; 304:110–115. [PubMed: 15064421]
56. Maupin P, Pollard TD. Improved preservation and staining of HeLa cell actin filaments, clathrin-coated membranes, and other cytoplasmic structures by tannic acid-glutaraldehyde-saponin fixation. The Journal of cell biology. 1983; 96:51–62. [PubMed: 6186673]
57. Willingham MC, Rutherford AV. The use of osmium-thiocarbohydrazide-osmium (OTO) and ferrocyanide-reduced osmium methods to enhance membrane contrast and preservation in cultured cells. J. Histochem. Cytochem. 1984; 32:455–460. [PubMed: 6323574]
58. Suloway C, et al. Automated molecular microscopy: the new Leginon system. J. Struct. Biol. 2005; 151:41–60. [PubMed: 15890530]

59. Scheffer LK, Karsh B, Vitaladevun S. Automated alignment of imperfect EM images for neural reconstruction. 2013
60. Cardona A, et al. TrakEM2 software for neural circuit reconstruction. PLoS One. 2012; 7:e38011. [PubMed: 22723842]
61. Schindelin J, et al. Fiji: an open-source platform for biological-image analysis. Nat Methods. 2012; 9:676–682. [PubMed: 22743772]
62. Dellovade TL, et al. Disruption of the gene encoding SF-1 alters the distribution of hypothalamic neuronal phenotypes. J. Comp. Neurol. 2000; 423:579–589. [PubMed: 10880989]
63. Betley JN, Cao Zhen Fang H. Ritola Kimberly D. Sternson Scott M. Parallel, Redundant Circuit Organization for Homeostatic Control of Feeding Behavior. Cell. 2013; 155:1337–1350. [PubMed: 24315102]
64. Wojcik SM, et al. An essential role for vesicular glutamate transporter 1 (VGLUT1) in postnatal development and control of quantal size. Proc. Natl. Acad. Sci. U. S. A. 2004; 101:7158–7163. [PubMed: 15103023]
65. Moechars D, et al. Vesicular glutamate transporter VGLUT2 expression levels control quantal size and neuropathic pain. J. Neurosci. 2006; 26:12055–12066. [PubMed: 17108179]
66. Betley JN, et al. Stringent specificity in the construction of a GABAergic presynaptic inhibitory circuit. Cell. 2009; 139:161–174. [PubMed: 19804761]

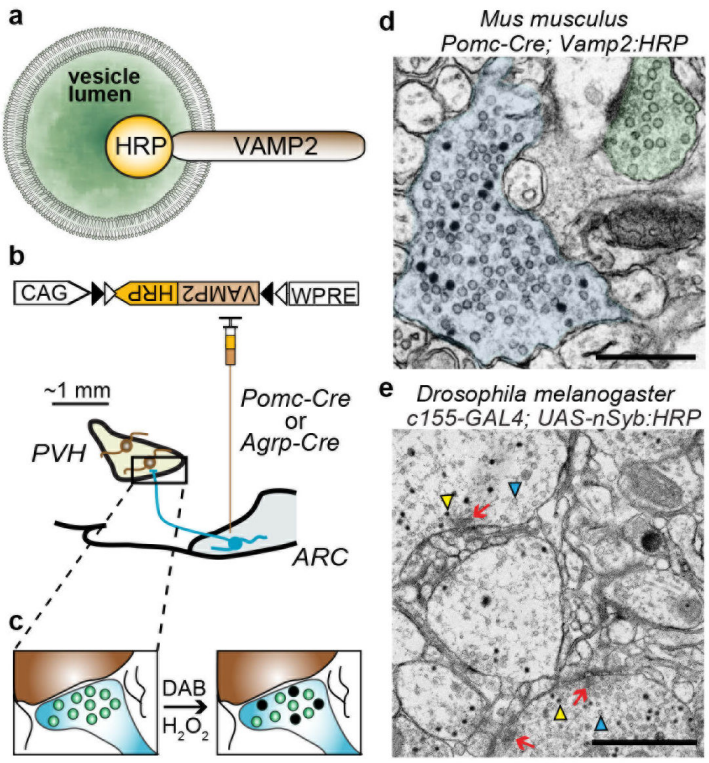

Figure 1. A genetically encoded synaptic EM marker for cell type-specific connectomics

a, Diagram of HRP targeted to the synaptic vesicle lumen by C-terminal fusion to VAMP2. **b**, (Above) rAAV2/1-*CAG-FLEX-rev-Vamp2:HRP*, a Cre-dependent viral vector for *Vamp2:HRP*. CAG: CMV enhancer/β-globin chimeric promoter, WPRE: woodchuck hepatitis virus posttranscriptional regulatory element, triangles: heterotypic loxP sites configured for Cre-dependent stable inversion of *Vamp2:HRP*. (Below) schematic for viral transduction and GESEM-labeling of POMC or AGRP neural circuit projections to the paraventricular hypothalamus (PVH). **c**, Schematic of DAB polymerization in VAMP2:HRP-expressing vesicles. **d**, Electron micrograph showing electron-dense DAB-labeled (blue) and unlabeled (green) boutons. Scale, 0.5 μm. **e**, Electron micrograph from a transgenic *Drosophila melanogaster* (*c155-GAL4;UAS-nSyb:HRP*) brain with broad neuronal expression of vesicular lumen targeted HRP, which is tagged to the C-terminus of neural synaptobrevin (nSyb). Yellow arrowhead, example of labeled synaptic vesicle. Blue arrowhead, example of unlabeled synaptic vesicle. Red arrow, T-bar structure that indicates a synaptic contact in *Drosophila melanogaster*. Scale bar, 1 μm.

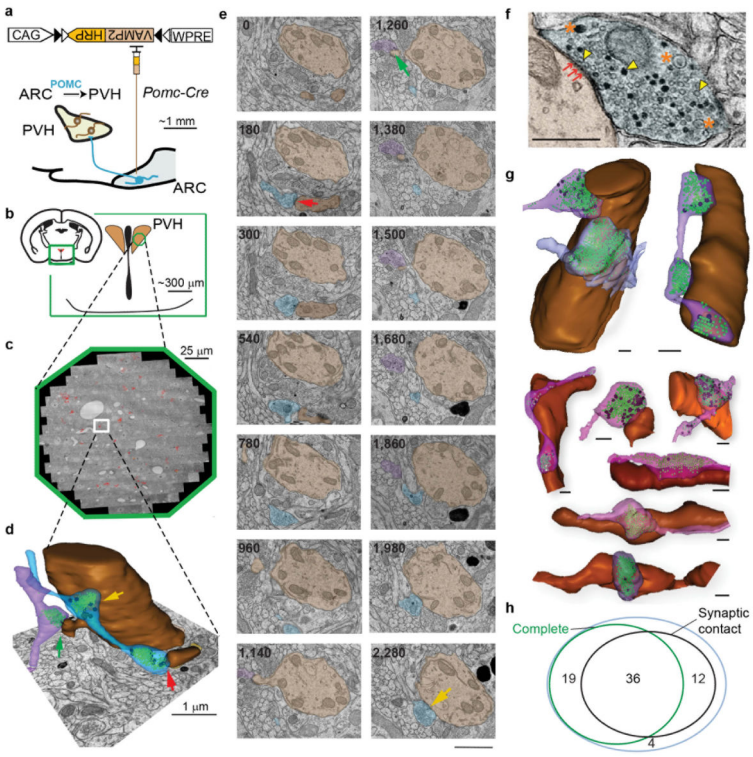

Figure 2.

GESEM-labeling for identification and reconstruction of ARC$^{POMC}\rightarrow$PVH circuits. **a**, Schematic drawing for targeting Cre-dependent rAAV to POMC neurons for VAMP2:HRP expression **b**,**c**, Location (**b**) and aligned electron micrographs (**c**) of imaged PVH area from a mouse brain expressing VAMP2:HRP in POMC neurons (red: DAB-labeled boutons from one *POMC-Cre* mouse). **d**, Two reconstructed ARC$^{POMC}\rightarrow$PVH axon segments (purple and blue) (Green: SVs, Black: LVs) making synaptic contacts (arrows) with a dendrite and a spine in the PVH (brown). **e**, Multiple z-aligned electron micrographs for the reconstructed terminals in **d** (numbers at upper left indicates position in z-axis in nanometers, based on 60 nm section thickness). Arrows, synaptic contacts. Scale, 1 μm. **f**, Example electron micrograph illustrating a synaptic contact (arrows) as well as labeled and unlabeled SVs (arrowheads) and LVs (asterisks). Scale, 0.5 μm. **g**, Other example ARC$^{POMC}\rightarrow$PVH bouton reconstructions. Green: SVs, Black: LVs. Scale, 0.5 μm. **h**, Venn diagram of all boutons containing DAB-labeled vesicles categorized for completeness within the imaged volume and the presence of a post-synaptic partner. Most labeled boutons resided completely within the imaged volume (77%), and the majority (68%) of the boutons from POMC neurons had ultrastructural characteristics of a synaptic contact.

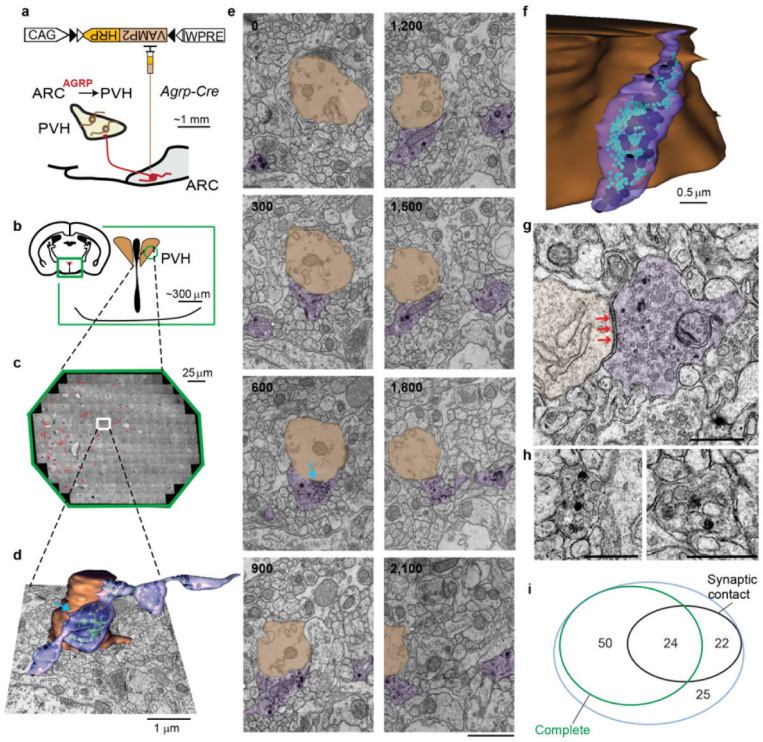

Figure 3. GESEM-labeling for identification and reconstruction of ARC^{AGRP}→PVH circuits

a, Schematic for viral transduction of AGRP neural circuits with VAMP2:HRP. **b**,**c**, location (**b**) and aligned electron micrographs (**c**) of imaged PVH area from a mouse brain expressing VAMP2:HRP in AGRP neurons (Red: DAB-labeled boutons from one *Agrp-Cre* mouse). **d**, Example reconstructed AGRP axonal release site (purple) with small and large vesicles (Green: SVs; Black: LVs) making synaptic contact (arrow) with a dendrite in the PVH (brown), overlaid on top of an electron micrograph. **e**, Electron micrographs for the reconstructed terminal in (**d**), with multiple images (numbers at upper left indicates position in z-axis in nanometers, based on 60 nm section thickness). Arrow, synaptic contact. Scale, 1 μm. **f**, Example reconstruction of an AGRP terminal making synaptic contact with PVH neuron soma (Green: SVs, Black: LVs). **g**,**h**, Electron micrograph of a mixed SV/LV release site with a synaptic contact (**g**) (red arrows) and predominantly LV-containing boutons that are non-synaptic (**h**). Scale, 0.5 μm. **i**, Venn diagram of all boutons containing DAB-labeled vesicles categorized for completeness within the imaged volume and the presence of a post-synaptic partner. The majority of boutons (62%) were complete within the imaged volume, and 32% of identified boutons had a synaptic specialization with a clearly identifiable post-synaptic partner.

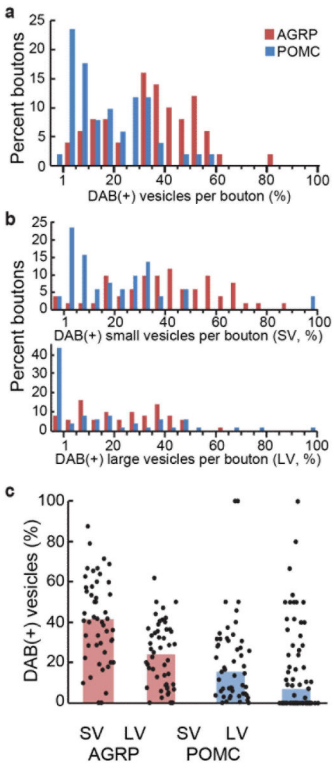

Figure 4. Penetrance for VAMP2:HRP DAB-labeling of synaptic vesicles

a, Distribution for percentage of DAB-labeled vesicles in reconstructed boutons (LV+SV for AGRP and POMC neurons). **b**,**c**, Histogram with percentage of DAB-labeled small (SV, top) and large vesicles (LV, bottom) (**b**) and median values (**c**) overlaid with the values obtained from individual boutons. (For AGRP: n = 51 boutons from one mouse, for POMC: n = 51 boutons from one mouse).

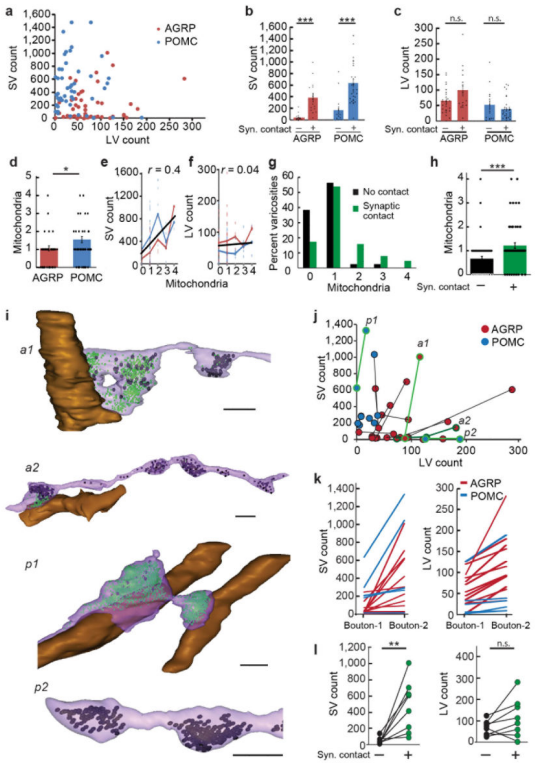

Figure 5. Quantitative intra-axonal organelle profile of ARC^{AGRP}→PVH and ARC^{POMC}→PVH boutons

a, Number of SVs plotted against LVs for each bouton. **b**,**c**, Number of SVs and LVs for each bouton with respect to presence of a postsynaptic contact site. (**b**) Small vesicles. AGRP non-synaptic: 38.2 ± 9.4, n = 27, AGRP synaptic: 365 ± 52, n = 24, U-test, $U = 17.5$, $P < 0.001$; POMC non-synaptic: 43.1 ± 11.3, n = 11, POMC synaptic: 650 ± 77.3, n = 40, U-test, $U = 0.0$, $P < 0.001$. n = 1 mouse each. (**c**) Large vesicles. AGRP non-synaptic: 62.2 ± 7.2, n = 27, AGRP synaptic: 86.1 ± 12.9, n = 24, U-test, $U = 261.5$, $P = 0.24$; POMC non-synaptic: 61.6 ± 17.4, n = 11; POMC synaptic: 30.5 ± 5.0, n = 40, U-test, $U = 168.5$, $P = 0.24$. n = 1 mouse each. **d**–**f** Number of mitochondria in each bouton with respect to cell type (**d**) (AGRP: 0.83 ± 0.1; POMC: 1.23 ± 0.14, n = 51 boutons each, n = 1 mouse each; U-test, $U = 1007.5$, $P = 0.03$), SV (**e**), and LV (**f**) counts. Red, AGRP. Blue, POMC. Black, regression line. **g**,**h**, Distribution (**g**) and mean number (**h**) of mitochondria in each bouton with respect to the presence of a postsynaptic partner (non-synaptic: 0.77 ± 0.12 mitochondria, n = 43 boutons; synaptic: 1.3 ± 0.15 mitochondria, n = 47 boutons; pooled from one *Agrp-Cre* and one *Pomc-Cre* mouse, U-test, $U = 689.5$, $P = 0.005$). **i**, Example reconstructions of axonal segments with multiple GESEM-labeled boutons. *a1* and *a2*: AGRP axons with multiple boutons, one makes a synaptic contact and the others are non-synaptic and contain mostly LVs. *p1*: A POMC axon making two synaptic contacts onto two dendritic segments. *p2*: A POMC axon with two boutons filled with LVs and no apparent SVs or postsynaptic contacts. Scale, 1 μm. **j**, SV and LV numbers in individual boutons, where boutons that are on the same axonal segment are connected with a line. Green highlight: axons reconstructed in (**i**). **k**, Vesicle numbers in adjacent boutons can be dramatically different for SVs (left) but LV numbers are usually similar (right). **l**, From

$ARC^{AGRP}\rightarrow$PVH axons, SV and LV numbers in adjacent boutons with respect to the presence of a postsynaptic element (small vesicles, non-synaptic: 48.8 ± 14.8, synaptic: 479.6 ± 112, paired t-test, $t(7) = -3.77$, $P = 0.007$; large vesicles, non-synaptic: 69 ± 11.9, synaptic: 115.9 ± 32, paired t-test, $t(7) = -1.82$, $P = 0.11$; n = 8 AGRP axonal segments from one mouse). Values are mean ± s.e.m. n.s. $P > 0.05$, $^{*}P < 0.05$, $^{**}P < 0.01$, $^{***}P < 0.001$.

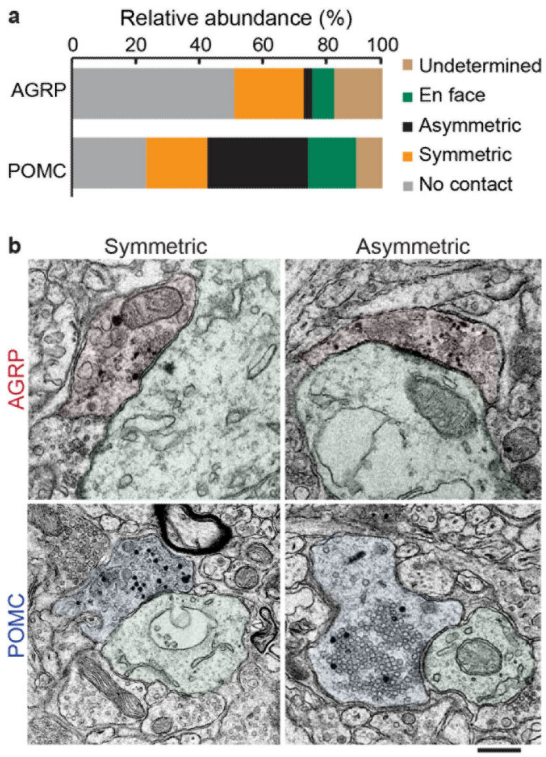

Figure 6. Postsynaptic profile of molecularly defined ARC→PVH projections

a, Quantitative analysis of GESEM-labeled boutons with respect to the morphology of postsynaptic elements (see Methods) (For AGRP: n = 121 boutons from one *Agrp-Cre* mouse; for POMC: n = 71 boutons from one *Pomc-Cre* mouse). **b**, Electron micrographs for ultrastructural subtypes of GESEM-labeled synapses in the PVH. Postsynaptic elements are shaded green. Scale, 0.5 μm.